Simultaneous Type-I/Type-II Emission from CdSe/CdS/ZnSe Nano-Heterostructures

Udit Soni,[†] Anuushka Pal,[†] Sajan Singh,[†] Mona Mittal,[†] Sushma Yadav,[†] Ravikrishnan Elangovan,[‡] and Sameer Sapra[†,*]

[†]Department of Chemistry, Indian Institute of Technology Delhi, Hauz Khas, New Delhi 110016, India, and [‡]Department of Biochemical Engineering and Biotechnology, Indian Institute of Technology Delhi, Hauz Khas, New Delhi 110016, India

ABSTRACT Core/intermediate/shell (C/I/S) structures with Type-I emission are well-known and are gaining immense importance due to their superior luminescence properties. Here, we report a unique C/I/S structure composed of CdSe/CdS/ZnSe that exhibits both Type-I and Type-II phenomena. The structures have been well characterized using a combination of optical and structural techniques. The photoluminescence (PL) and photoluminescence excitation (PLE) data indicate the formation of a combined Type-I and Type-II structure in one material, results supported by simple theoretical calculations. Single particle fluorescence reveals colocalization of both the emissions. The X-ray diffraction (XRD) and transmission electron microscopy (TEM) results confirm the structure of these particles. The time-resolved fluorescence studies show the possibility of tuning the lifetime of these materials by changing the Type-I/Type-II thickness ratios. It is possible to form these two separate excitons in the same system separated by a CdS intermediate layer that acts both as a barrier and an active member of the Type-II system allowing the generation and recombination of two excitons, in violation of Kasha's rule.

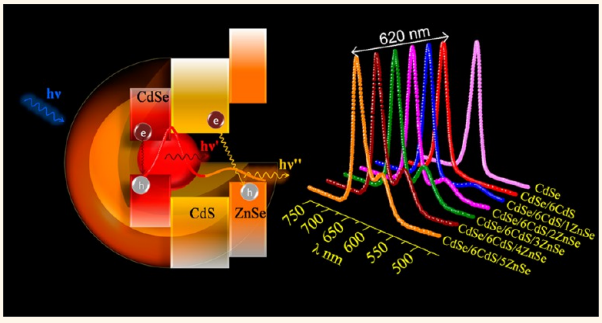

KEYWORDS: CdSe/CdS/ZnSe · Type-I/Type-II · dual emission · nanocrystals · C/I/S · SHNS

Recent advances in the development of nanomaterials for device fabrication technology,[1−3] biological markers[4] and sensing technology[5] have encouraged the search for synthetic methodologies that could offer better control over these material properties.[6] Therefore, it remains a main objective to develop efficient routes for the synthesis of high-quality, monodisperse, crystalline nanomaterials. Semiconductor hetero-nanostructures (SHNS) provide an alternative opportunity to engineer the required nanocrystal properties, by tailoring not only the size but also their composition.[7−11] They are therefore an important group of semiconducting materials for use in further advancements in the field of light emitting devices,[2] photovoltaics[1] and sensors.[12]

On the basis of relative alignment of the conduction band (CB) and valence band (VB) edges of the materials of the semiconductors, heterostructures are classified as Type-I or Type-II.[7] In the Type-I structures, both the CB and the VB edges of one semiconductor are situated within the energy gap of the other semiconductor, localizing the electron−hole pair in one semiconductor. These structures, particularly those with a direct band gap, as a result have an efficient radiative recombination, which makes them useful in biological labeling and LEDs.[2,4] In the Type-II situation, the lowest energy states, CB and VB for electrons and holes, respectively, reside on different semiconductors. The electrons and holes are spatially separated in different regions of the heterojunction. These structures are useful in applications such as photovoltaic devices,[8,11,13,14] where it is necessary to separate the charge carriers before they can recombine.

By the use of core/shell design, it has been possible to synthesize both Type-I and Type-II systems.[8,13,15−21] Further addition of a shell, thereby fabricating a core/intermediate/shell (C/I/S) system, has been possible by the successive ion layer adsorption and reaction (SILAR) technique reported by Peng *et al.*[22]

* Address correspondence to sapra@chemistry.iitd.ac.in.

Received for review May 8, 2013 and accepted November 27, 2013.

Published online November 27, 2013
10.1021/nn404537s

Following this, they also published a report on the synthesis of dual emitters *via* successive injection of air stable precursors, where they synthesized core/barrier/shell type nanocrystals of CdSe/ZnS/CdSe, which is a Type-I/Type-I emitter from the CdSe core and a thinner CdSe shell separated by a ZnS barrier layer.[22,23] Other reports have also been published on similar systems.[18,24−28] Despite well-established synthesis routes for Type-I/Type-I nanocrystals,[18,23] only a few reports exist on the formation of Type-II/Type-I,[9,15] and of Type-I/Type-II[11] heterostructures. To the best of our knowledge, only one report is available on SHNS based on CdSeTe/CdS/ZnCdSe having a Type-I/Type-II structural arrangement with distinguishable optical properties from both domains.[29]

Here, we report the colloidal synthesis of CdSe/CdS/ZnSe Type-I/Type-II system in a single nanocrystal (NC) showing dual emission from both systems, a fact also verified using single particle fluorescence measurements. The emissions from CdSe/CdS and CdS/ZnSe in the CdSe/CdS/ZnSe nanocrystals are termed as core and shell emissions, respectively, in the following discussion. A simple theoretical model based on the effective mass approximation shows the core emission arising from the electrons and holes localized in the CdSe layer, whereas the shell emission is a result of recombination from the electrons localized on the CdSe and CdS layers and the hole residing on the outer ZnSe layer.

RESULTS AND DISCUSSION

The bulk band edge alignments of the three materials used in this work, namely, CdSe, CdS, and ZnSe, are shown in Figure 1. The band-gaps and band edge locations of CdSe, CdS, and ZnSe have been taken from previous reports.[7,30,31] Such a system has been chosen to ensure a Type-I heterostructure composed of CdSe/CdS and a Type-II heterostructure due to CdS/ZnSe. The synthesis of this C/I/S system starts with the synthesis of CdSe nanocrystals followed by overcoating the intermediate CdS shells of various thicknesses. The procedure is mentioned in the section on methods, while the absorption and photoluminescence (PL) spectra of CdSe core and CdSe/CdS nanocrystals are shown in Figure S1 (see Supporting Information). The CdSe/CdS core nanocrystals were named as CdSe/*m*CdS, where *m* is the number of monolayers. A significant red-shift was observed in the absorption and PL spectra of the CdSe/mCdS nanocrystals with increasing shell thickness, *i.e.*, *m* varying from 1 to 6, indicating substantial delocalization of the charge carrier wave functions into the CdS layers, a well-established fact[22,32,33] and also supported by the theoretical calculations reported below showing mainly the delocalization of the first electronic wave function in the CdS layers.

For coating the outer ZnSe layer, the system with the largest CdS intermediate shell, CdSe/6CdS, was chosen.

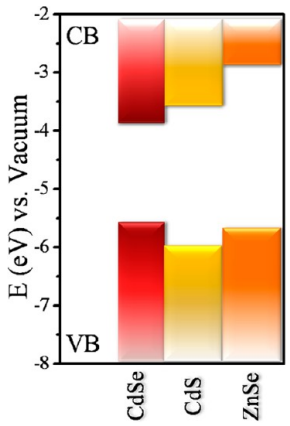

Figure 1. Relative band alignment of bulk CdSe, CdS and ZnSe.

It is known that large separations between the inner core material and the outermost shell enable a decoupling of the electronic shell in such C/I/S systems.[23] The UV−visible absorption and fluorescence (λ_{ex} = 377 nm) spectra of the CdSe/6CdS/nZnSe are shown in Figure 2, panels a and b, respectively. As the thickness of the ZnSe shell was increased from n = 1 to n = 5, no shift was observed in the first excitonic absorption peak of the CdSe/6CdS core nanocrystals, which remains at 608 nm, but there was some increase in the absorption value at the higher energy side of the absorption spectra of the CdSe/6CdS/nZnSe nanocrystals, which developed with the growth of the ZnSe shell as seen in Figure 2a. The PL spectra of CdSe/6CdS/nZnSe C/I/S heterostructures differ considerably from those of CdSe/6CdS nanocrystals. There are two gross aspects that are seen: (a) the appearance of another feature at higher energy and (b) the change in the fluorescence intensity from the core CdSe/6CdS system. The growth of ZnSe shells on CdSe/6CdS nanocrystals results in two peaks in the PL spectra, both of which are sharp and distinguishable. This implies that two separate excitons are formed: one in the CdSe/6CdS and another due to CdS/nZnSe. The peak at lower energy is assigned to the core emission and the new peak at higher energy arises upon addition of the ZnSe shell and is therefore assigned to the shell emission. PL intensities are normalized to the absorption value at the first excitonic peak from CdSe/6CdS, essentially normalizing with the concentration of the CdSe/6CdS QDs as the first excitonic peak intensity is related to the concentration of the nanocrystals,[35] so as to obtain a quantitative estimate of the emission intensities with varying thickness of the ZnSe shells. For the CdSe/6CdS/nZnSe system, the data indicate that the core emission always has higher quantum efficiency than the shell emission. The electron−hole interaction seems to be much stronger in core-localized excitons than that in the shell-localized excitons, as has been shown earlier for the

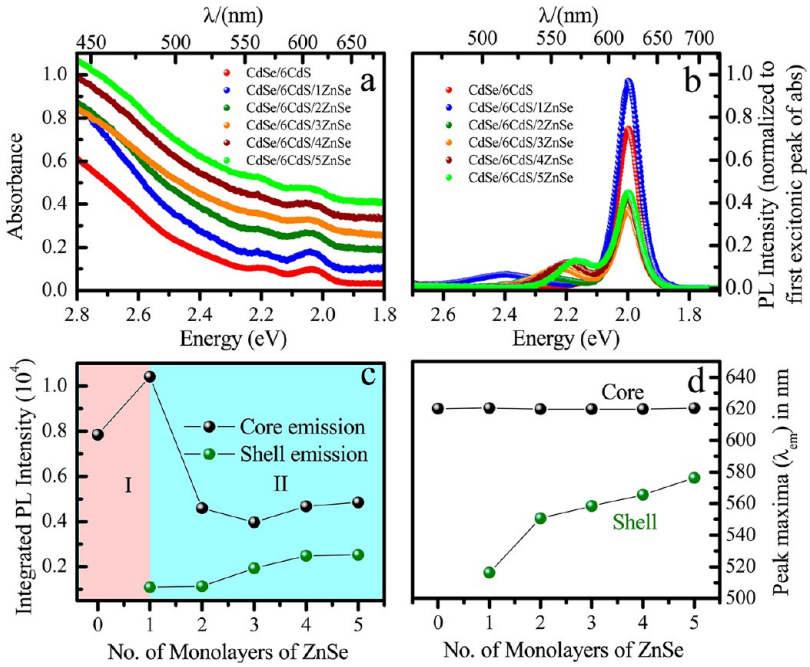

Figure 2. (a) UV−vis and (b) fluorescence spectra of CdSe/6CdS and CdSe/6CdS/nZnSe (n = 1−5), (c) change in integrated fluorescence intensity of core and shell emission, and (d) change in fluorescence peak position of core and shell emissions. Note that the absorption spectra have been vertically shifted for clarity. Conversion from wavelength to energy scale has been carried out using a Jacobian transformation.[34]

TABLE 1. List of Material Parameter for Calculations

	thickness (nm)	band gap (eV)	CBO with respect to CdSe (eV)	VBO with respect to CdSe (eV)	effective mass of electron m_e^*/m_e	effective mass of hole m_h^*/m_e
CdSe	1.75	1.74	-	-	0.13	0.5
CdS	2.10	2.40	0.24	0.42	0.21	0.7
ZnSe	1.33	2.70	0.89	0.07	0.17	0.6

case of CdSe/ZnS/CdSe, a core/barrier/shell system exhibiting Type-I/Type-I dual emission.[36]

To assign the two emissions observed in Figure 1b, we carried out simple calculations based on the effective mass approximation, explained in details previously.[18,25,26,36−40] For our theoretical calculations, we consider our system as spherically symmetrical, having CdSe core, enclosed by CdS and ZnSe layers. All the parameters used for the simulations are listed in Table 1 and have been adopted from literature.[31,40]

Figure 3a(i) and 3a(ii) show the first and second excited state probabilities for the electron and the hole, respectively. For n = 1 state most of the hole is localized in CdSe core, but the electron is distributed mainly in CdSe and a portion tunnels into the CdS layer. The n = 2 is a charge separated state where the electron is distributed in CdSe/CdS and the hole is distributed in ZnSe shell. Emission is expected from regions where the electron−hole overlap is the maximum. This, as shown in Figure 3a(iii), suggests the emission from the first excited state occurs largely within the CdSe core, while the emission from the second excited state occurs in the CdS/ZnSe shell, the electron coming from CdS and the hole residing in the ZnSe layer. Thus, we

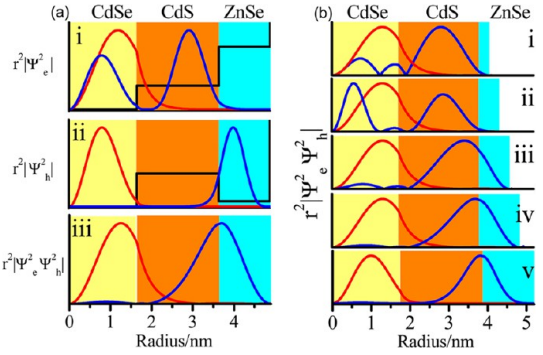

Figure 3. (a) Radial probability distribution functions for (i) electrons, (ii) holes and (iii) electron−hole overlap. Dark black line in panels I and ii represents bulk band alignment for hole and electron, respectively. (b) Evolution of the electron−hole wave function overlap as a function of the ZnSe shell thickness, (i) 1 ML, (ii) 2 ML, (iii) 3 ML, (iv) 4 ML and (v) 5 ML ZnSe shells. Red and blue color coding of wave functions is for n = 1, l = 0, m = 0 and n = 2, l = 0, m = 0, respectively.

can assign the core emission as Type-I while the shell emission as Type-II. It must be noted that such simple calculations cannot exactly pinpoint the exact emission centers, but they do grossly tell us the regions

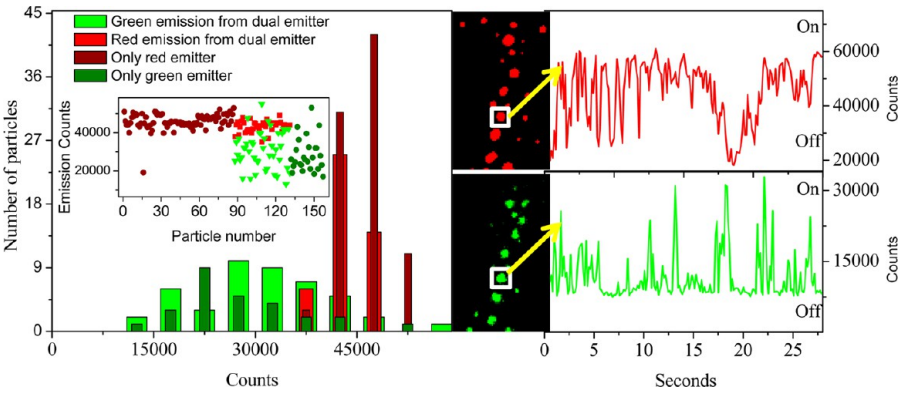

Figure 4. Left panel shows the number of particles histogram that show background subtracted only red, only green, and dual emission out of a total of 157 particles sampled. The inset shows the background subtracted emission counts for individual particles. Representative blinking traces (on/off states) for a single SHNS selected from the images shown in the middle panel are plotted in the right most panels, upper panel for core emission and lower panel for shell emission.

involved in the two emissions. Further, as we observe emission from the second excitonic peak, it is evident from the above calculations that this higher energy emission observed here is a violation of Kasha's rule, as has been observed for the CdSe/ZnS/CdSe dual emitter earlier.[29,41] However, we do not claim direct emission from the higher energy states. Rather it is most likely mediated *via* the traps, since it is well-known that carrier cooling is a rather fast process, which gets slowed-down in these systems.[25,36,38,39,41] Another striking feature is the fact that upon ZnSe overcoating, the core emission energy does not change at all. This implies the outer ZnSe layer is not affecting the electronic gap of the inner CdSe/CdS core. The results in Figure 3b show the electron−hole wave function overlaps for varying ZnSe shell thickness. As seen in the figure, the first excited state overlap function does not change at all upon changing the ZnSe shell thickness. In fact, the energy values for the electron and hole in the first excited state remain constant for any ZnSe thickness at 0.25 eV above the bottom of the conduction band and 0.14 eV below the top of the valence band, respectively.

As a direct evidence of dual emission, single particle fluorescence spectroscopy for our model system is carried out. All the experiments were conducted in air by spreading a very dilute solution of nanocrystal on to a freshly cleaned glass slide. The experimental details are given below in the Methods section. The right panel in Figure 4 shows the blinking traces for core and shell emission from a single nanocrystal; this blinking phenomenon is characteristic of single dot as reported previously.[25,42,43] A video of the blinking particles is also shown as part of Supporting Information. A statistical analysis to calculate the exact number of dual emitting particles was performed. Particles exhibiting complete on/off fluorescence intensity relative to background are considered as a single nanocrystal and are used in our statistical analysis, *i.e.*, particles that do not come down to the background level are not sampled as they are probably not single particles. In all, 157 particles were analyzed. The results are presented in the left panel of Figure 4 as histograms with intensity bin of 5000 counts. The inset also shows the intensity from individual blinking nanostructures. Among all the analyzed particles, about 28% of them are dual emitting, while 56% of them are emitting only as core and rest of them 16% are emitting only as shell. A considerable fraction are dual emitters and there is a large fraction that does not get overcoated by the shell. Also, separate nuclei of CdS yield CdS/ZnSe islands that emit only in the green channel. Although the red emission intensities are almost the same for all the single particles, the green intensities do have a large spread and this could perhaps be attributed to the partial coverage of the surfaces instead of complete monolayer coverage, which is also evident in the transmission electron microscopy (TEM) results shown below. Taking average of the emission intensities, one can calculate the red/green emission ratio to be 2.8, very close to the ensemble measured value of 3.3. The values are pretty close and the differences are due to the finite sample size and the use of filters that cut off certain emission wavelengths. Thus, one can be certain that the dual emitters are formed.

The reason we chose to work with six monolayers of CdS is to provide a large insulation barrier between the CdSe core and ZnSe shell. To examine the effect of thickness of CdS layers between CdSe core and ZnSe shell, C/I/S heterostructures with varying numbers of monolayers of CdS were synthesized. The plot in Supporting Information Figure S2 reveals that with two monolayers of CdS no emission from the shell is observed, but when the thickness of CdS is more than two monolayers, some feature of the shell emission appeared at the higher energy side. These results are consistent with earlier reports for the core/barrier/shell systems, stating that the degree of interaction of two quantum systems depends on the thickness of barrier layer and the barrier layer should be more than two

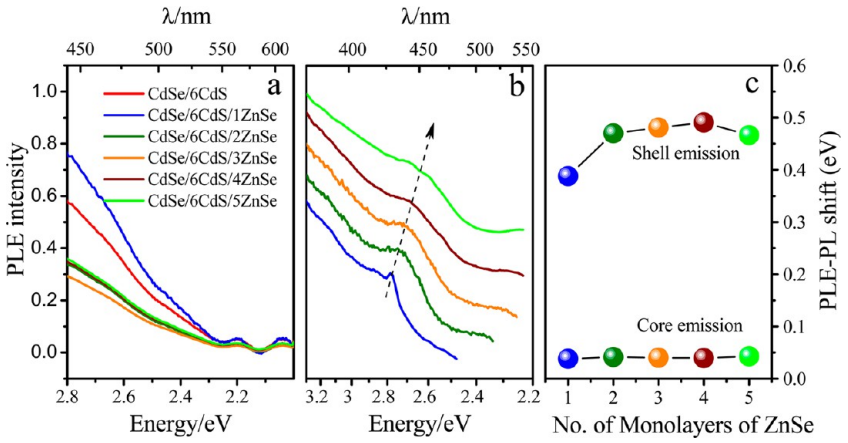

Figure 5. (a) PLE spectra of core emission, (b) PLE spectra of shell emission, and (c) variation in PLE−PL shifts for the core and the shell emissions. The same color codes are used for the three panels.

monolayers to observe emission from two quantum systems.[23,36,44,45] In the present system, the CdS layer between CdSe and ZnSe is not only working as barrier but also participating in the formation of Type-II system with outer ZnSe shell within the heterostructures. The position of the core peak remains unaltered on addition of ZnSe onto CdSe/6CdS. This is observed for all the CdSe/mCdS/nZnSe systems where *m* ranges between 2 and 6 and *n* from 1 to 5 (Supporting Information Figure S2). These results also confirm that the appearance of shell emission does not affect the core emission. Due to the well separated core and shell emissions, we have chosen CdSe/6CdS/nZnSe as a model system for our studies here: the core emission is of Type-I, while the shell emission is of Type-II.

The intensity of emission from the CdSe/6CdS core was observed to vary nonmonotonously with the addition of ZnSe shell as seen in Figure 2c. The changes in the intensity can be divided into two regions: region I shows an increase in intensity brought about after addition of one ZnSe shell, whereas region II exhibits a diminished intensity upon addition of more ZnSe shells. The increase of the emission intensity in region I could be attributed to the formation of a quasi-Type-II structure of CdS/ZnSe which is essentially similar to the Type-I electronic structure because of the large band gap of the thin ZnSe shell.[8] The subsequent decrease in the emission intensity with the growth of the shell is due to the formation of pure Type-II system of CdS/ZnSe. These results are in agreement with the report by Klimov and co-workers who reported the switchover from quasi Type-II to pure Type-II structures in the case of CdS/ZnSe nanocrystals.[8] If the ZnSe shell of CdS/ZnSe system is thin, the hole wave function is delocalized over the entire nanocrystal. This situation leads to partial charge separation (quasi Type-II regime) in which the electron is confined to the CdS layer.[8] This gives a scenario where the exciton generated in the CdS/ZnSe part can also go over to CdSe as CdS/ZnSe effectively forms a large band gap outer-layer. This is also evident from the calculations seen in Figure 3b(i). So, in region I, both shells, CdS as well as ZnSe, help in confining the excitons into the CdSe core, resulting in a higher intensity from the core. However, with thicker ZnSe shell, the system moves into a true Type-II regime, where the hole wave function is confined into the ZnSe shell. The excitons created in the shells are now far separated from those of the core, resulting in the reduction of core emission and an increment as well as red-shift in the shell emission with the growth of ZnSe shell, seen in Figure 2d. Thus, regions I and II in our system are the result of transition from an initial quasi Type-II to a Type-II arrangement. Another possibility that could be responsible for this two-region behavior is the lattice mismatch between the CdS and ZnSe layers which would increase as the ZnSe shell thickness increases.

Photoluminescence excitation (PLE) technique is used to distinguish between several emitting species that might have separated emission wavelengths but whose absorption features overlap with each other. Figure 5 shows the PLE spectra of the C/I/S SHNS for both the core and shell emissions. The PLE spectra of the core emission peak for all CdSe/6CdS/nZnSe samples, including CdSe/6CdS, are shown in Figure 5a. The PLE spectra of core emissions follow the same trends like the absorption spectra exhibiting the first and second excitonic peaks without any shifts. In Figure 5b, the PLE spectra (shifted for clarity) of the high energy shell emission show a distinguishable feature at a higher energy for a new excitation channel, which corresponds to the typical CdS/ZnSe system; the spectral features for such a system are presented in Supporting Information Figure S3. This feature is present in all CdSe/6CdS/nZnSe systems and is gradually red-shifted and gets broadened with increasing thickness of ZnSe as seen in Figure 5b. So the absorption spectrum of the CdSe/6CdS/nZnSe system is the sum of the two excitation channels present in the same entity. The PLE-PL shifts for core and shell emissions were calculated from the difference between the

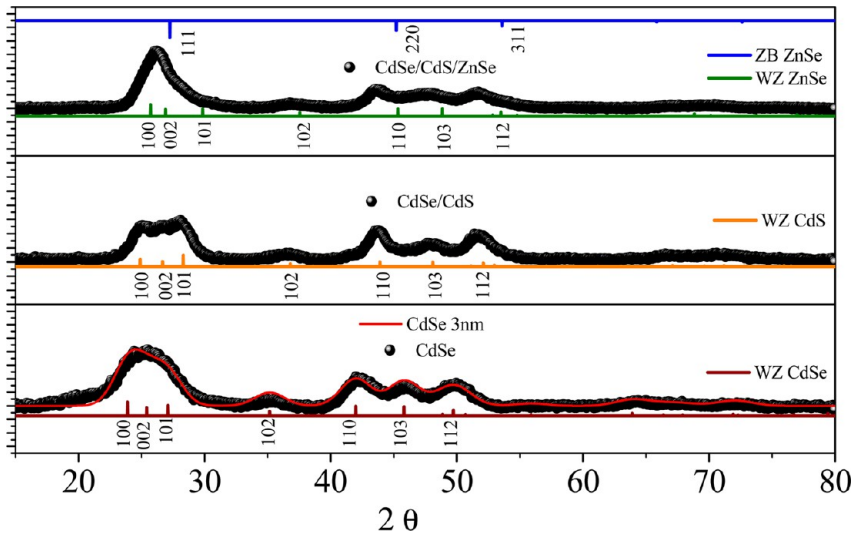

Figure 6. Powder XRD patterns of CdSe, CdSe/6CdS and CdSe/6CdS/5ZnSe. The red line shows the bulk-broadened pattern for wurtzite CdSe.

excitation and emission peaks[46,47] and are plotted in Figure 5c. The shifts for core emission remains almost constant (≈ 0.04 eV) with increasing shell thickness. These low values are typical for the Type-I systems.[48] But the difference in the PLE peak and PL peak values for shell emissions is much higher (between 0.38 to 0.49 eV), typical for a Type-II system.[19] The steady increase of these PLE-PL shifts upon shell growth of ZnSe is also observed, reaching up to 0.49 eV for thick ZnSe shells. These results also support that the core exhibits Type-I nature while shell has Type-II nature. The origin of the Type-II emission from the CdS/ZnSe shells of CdSe/CdS/ZnSe is the radiative recombination of the electron−hole pair across their interface. Here, the energy of Type-II emission depends on the band offsets of the CdS and ZnSe. Type-II systems can thus emit at energies that are smaller than the band gap of either material, CdS and ZnSe in the present case. Hence, the Type-II system shows higher values of the PLE-PL shifts.[19]

Further support of the fact that we have formed the heterostructures comes from the structural characterizations. Figure 6 shows powder X-ray diffraction (XRD) patterns of representative samples of CdSe, CdSe/6CdS and CdSe/6CdS/5ZnSe systems together with their diffraction patterns of the bulk materials obtained from the JCPDS database. Figure 6 shows that the crystal structure of the prepared CdSe seeds can be assigned to a typical wurtzite structure with the presence of its characteristic reflections and the experimental diffraction patterns of the CdSe are well matched with broadened pattern obtained using the Scherrer equation[49] shown as the red line in the Figure 6. The best fit gives an estimate of 3 nm CdSe nanocrystals which is in good agreement with the size obtained from the absorption spectrum. The addition of CdS shell caused a small shift in the diffraction peak of nanocrystals to the higher reflection angles due to its smaller lattice constant compared to wurtzite CdSe[17,33] which indicates a presence of both CdSe and CdS in the structure.[17,50] As expected from the bulk diffraction pattern, the deposition of ZnSe causes diffraction peaks to shift toward higher angles with respect to those in CdSe/CdS due to smaller lattice parameters of the ZnSe. The peaks corresponding to CdSe/CdS and ZnSe, however, cannot be well distinguished and separated. Instead the observed pattern is characterized by a rather uniform broadening of diffraction features. Three peaks should appear at around 29°, 45.34° and 53.5° 2θ values for ZnSe. Thus, the broadened diffraction was observed at those positions which is described by the deposition of ZnSe as was previously reported for CdS/ZnSe nanoparticles.[8,15] Careful observation of this XRD pattern reveals that the peaks corresponding to (100) and (002) planes show a higher intensity compared to the other planes indicating that growth of ZnSe is not uniform but it is greater in particular directions which is further confirmed by TEM images discussed below. The ZnSe crystal phase could as well be zinc blende. It is rather certain that the ZnSe phase is WZ and not ZB by noting the XRD pattern at the (103) peak position. The (103) peak is characteristic of the WZ phase and absent in the ZB phase. The relative intensity of this peak with respect to (110) and (112) increases when ZnSe is added on top of CdSe/6CdS. If ZnSe had been in the ZB structure, the intensity of this part should have decreased instead.

Figure 7 shows representative TEM images of CdSe, CdSe/6CdS and resulting CdSe/6CdS/5ZnSe structures synthesized by overcoating with five monolayers of ZnSe. CdSe nanocrystals are nearly spherical with a narrow size distribution (core diameters d = 3.5 nm). The CdSe/6CdS have almost spherical as well as a

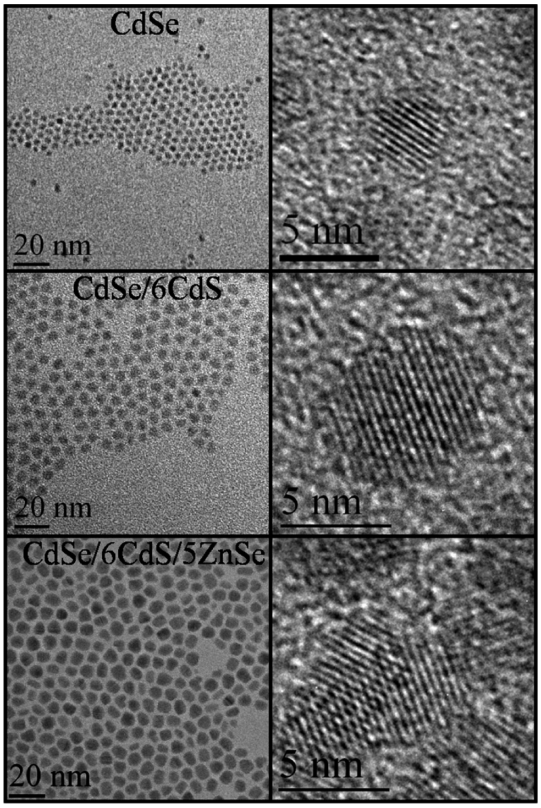

Figure 7. TEM (left) and HRTEM (right) images of representative CdSe, CdSe/6CdS and CdSe/6CdS/5ZnSe.

narrow size distribution with an increased average size (d = 7.1 ± 0.5 nm). No small particles were observed indicating the deposition of CdS on CdSe is homogeneous, which implies very small particles of CdS, not detectable here, may be present. Further overcoating of CdSe/6CdS with ZnSe makes these nanocrystals slightly irregularly spherical in shape and the size distribution broadens too. A similar irregularity in shape of ZnSe coated CdS nanocrystals has also been reported earlier.[8] An increase in the size (d = 8.3 ± 0.8 nm, l = 6 ± 0.6 nm) confirms the deposition of ZnSe. The origin of these irregular shapes is due to the preferential growth of particular planes of ZnSe; here the (100) and (002) planes of ZnSe are more elongated than the other planes. This could perhaps be the reason for the spread in intensity from the green emitting channel. A few very small particles are also observed in TEM of CdSe/6CdS/5ZnSe samples; the presence of these small particles indicate formation of islands of CdSe/CdS or ZnSe or CdS/ZnSe particles. These free CdS/ZnSe particles are responsible for the only green emitting particles. Some free ZnSe particles are also possible but their sizes should be much smaller than what we observe here. High-resolution TEM images on the right panels in Figure 7 of CdSe, CdSe/6CdS, and CdSe/6CdS/5ZnSe nanocrystals show lattice planes. Lattice planes for CdSe extend across the full particle length. HRTEM image of CdSe/6CdS show no clear evidence of an interface between CdSe and CdS, but a close investigation of edges of particles gives excellent information about the shell, which shows a diminished contrast compared to the core. In case of CdSe/6CdS/5ZnSe, crossed planes suggest an overcoating of a material on top the CdSe/6CdS structures indicating coverage by ZnSe. Even the extension of ZnSe along one direction confirms the anisotropic growth of ZnSe. The presence of the shell materials is further confirmed by the energy dispersive X-ray (EDX) analysis (see Supporting Information Figure S4). CdSe nanocrystals show the existence of Cd and Se and the appearance of strong signal for S in CdSe/6CdS confirms the presence of Cd and S. EDX spectrum of CdSe/6CdS/5ZnSe C/I/S nanocrystals shows characteristic peaks of Cd, Se, S and Zn.

The two emissions from the CdSe/CdS core and CdS/ZnSe shell decay through different channels. Lifetime measurements were carried out to investigate the fluorescence dynamics of the charge carriers of the dual emission from the core, core/shell and C/I/S systems. Previous reports[51] are available on the lifetime studies of Type-II nanostructures, which show that the lifetime of Type-II nanostructures is noticeably higher compared to that of Type-I systems due to separated charges. The decays measured here were all found to be multiexponential and could be adequately fit to a sum of two or three exponentials. The decay times with percentage contributions are listed in Supporting Information Table S1. Figure 8 shows typical decay curves for CdSe, CdSe/6CdS and CdSe/6CdS/nZnSe heterostructures recorded at room temperature. A general trend to be noted is that the average lifetime of the shell emission is higher than that of the core emission and increasing the shell thickness decreases the average shell lifetime, while it hardly affects the average core lifetime. These are discussed in detail here.

Decay trace of CdSe is fitted with three lifetime components of 0.69, 5.21, and 21.42 ns that have been assigned to deep traps, band edge recombination, and shallow trap assisted recombination, respectively.[52−54] After addition of CdS layers, the resulting measured decays are fitted with two lifetime components −3.54 and 17.78 ns, assigned to band edge and shallow trap state mediated processes, respectively. The excited electron shuttles between the band edge and these shallow trap states, and finally decays through the band edge, thereby increasing the lifetime to about tens of nanoseconds. The disappearance of shortest lifetime component from CdSe by the addition of CdS is known to be due to elimination of surface dangling bonds.[52,53] For CdSe/6CdS/nZnSe samples, the lifetime decays were collected for core and shell peaks. The two lifetime components (3.85 (±0.5) and 18.58 (±0.7) ns) of decay remain almost constant in core emission for all the CdSe/6CdS/nZnSe samples.

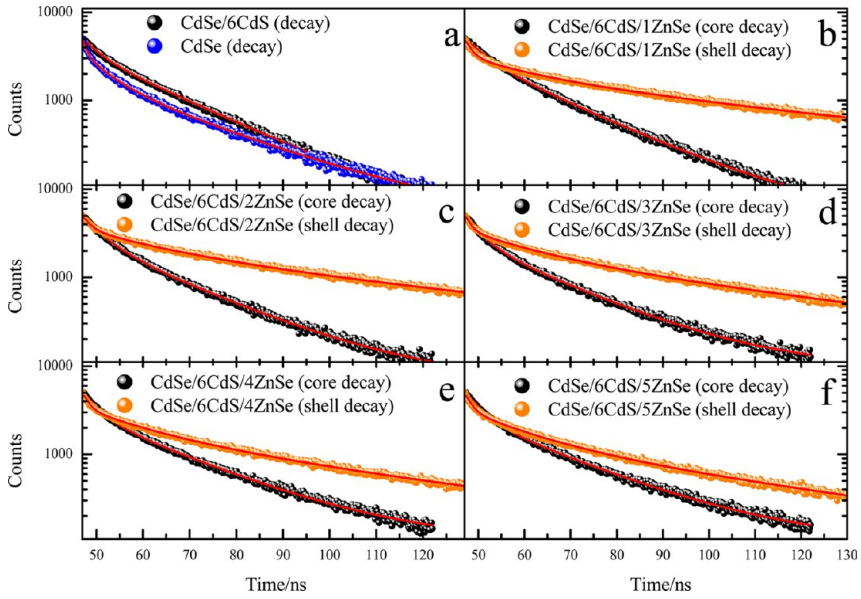

Figure 8. (a) Decay profiles for CdSe and CdSe/6CdS and (b−f) decay profiles for core and shell emissions from C/I/S systems. Red lines on each decay profile are the fitted curves.

Thus, the outer ZnSe shell does not affect the dynamics of the core emission.

Decay for shell emission of CdSe/6CdS/nZnSe can also be fitted with the sum of three lifetimes. In analogy to the case of bare nanocrystals,[52−54] the slowest lifetime component (~50 ns) is assigned to shallow trap states, the medium lifetime component (~13 ns) is ascribed to band edge decay, and the fastest component (~1.4 ns) is again attributed to the appearance of surface dangling bonds on the surface of outermost ZnSe layer, though more work needs to be carried out in order to confirm these assignments. We observed longer average lifetimes for these shell emissions compared to core emission for respective nanocrystals (see Supporting Information Table S1). The very short lifetime component of the higher emission from the shell decay might be an indication of some sort of energy transfer process occurring from the shell to the core as has been reported earlier in a similar system by Deutsch *et al.*[29] These exciton dynamic results are further supported by previous reports stating that for Type-II systems the wave function overlap between the excitons decreases because of spatial charge separation,[55] which results in longer radiative lifetimes. It is expected from literature that for each addition of ZnSe the lifetime of shell emission should increase,[51] but a surprising result found in our study is that by addition of one and two monolayer of ZnSe, the average lifetime of the shell emission increases from 24.67 to 27.70 ns as expected,[51] but further addition of ZnSe monolayer results in a considerable reduction of average lifetime of shell emission and finally it reached 17.36 ns for CdSe/6CdS/5ZnSe. Looking at the lifetime Table S1, the main contribution for this reductions is the long-lived component ($\tau_3 > 50$ ns). This reduction of lifetime indicates a new structural insight toward the CdS/ZnSe interface in the CdSe/6CdS/nZnSe ($n > 2$) systems. According to Eychmüller and coworkers, reduction of lifetime of CdS/ZnSe system is due to the alloying at the interface of CdS/ZnSe.[56] So in the present system, the interface of CdS/nZnSe (when $n \leq 2$) is initially well separated, but with the addition of more ZnSe monolayers, an increase in the size, as well as an alloying of the interface, is observed. When we closely investigated the lifetime component of shell decay with each addition of ZnSe, lifetime of fastest component was observed to remain almost same for all the samples because the nature of the outermost surface remained unchanged, whereas the lifetime for the slowest and medium components gradually decreased, which indicates the partial removal of shallow traps due to the alloying at the interface of CdS and ZnSe. This further confirms the proposed lifetime assignments. These results are also supported by excitation spectra of shell emission shown in Figure 5b. A close investigation of PLE spectra of shell emission reveals that the PLE spectral features are sharper in systems with one or two monolayers of ZnSe. One reason is the increase in polydispersity of the samples as more ZnSe layers are added. However, this cannot be the sole reason as the PL spectra are not so broad for these thicker ZnSe shell emissions. This smearing of the PLE peaks could also be due to excitation across the CdS/ZnSe band edges. After addition of more ZnSe monolayers, alloying occurs at the interface and these band edges get more diffused. Therefore, the PLE spectral features broaden due to the softening of a confinement at the interface.[57]

CONCLUSIONS

In summary, we have synthesized dual emitting C/I/S semiconductor nanocrystals consisting of a CdSe core

and a ZnSe outer shell separated by a CdS layer. The origin of the two emissions was investigated and it was found that they are from two different channels: one from the CdSe/CdS core which is a Type-I system and the other from CdS/ZnSe shell which is a Type-II system. These assignments are in agreement with simple theoretical calculations. Our results confirm that the CdS layer between the CdSe and ZnSe not only serves as a barrier for the Type-I and Type-II systems but also participates in forming the Type-II system with the outer ZnSe shell. These nanocrystals provide a single unit having charge separated as well as charge confined domains and are suitable candidates for multiexciton generation and single photon sources.

METHODS

Chemicals. Cadmium oxide (CdO, 99.5%), zinc oxide (ZnO, 99.5%), trioctylphosphine oxide (TOPO, 99%), trioctylphosphine (TOP, 99%), 1-octadecene (ODE, 90%), oleic acid (OA, 90%), sulfur powder (99.9%) and selenium powder mesh (99.99%) were purchased from Sigma-Aldrich. Octadecylamine (ODA, 97%) was purchased from Merck Chemicals. All the solvents were anhydrous and were purchased from Merck chemicals.

Characterization. UV−vis absorption spectra were acquired on Perkin-Elmer Lambda 1050 spectrophotometer. Dilute solutions of NCs in hexane were placed in four window 1 cm quartz cuvettes, and their absorption and corresponding fluorescence were measured. The fluorescence spectra were recorded on Perkin-Elmer LS-55 spectrometer with constant 5 nm excitation and emission slit width with an excitation wavelength of 377 nm. Transmission electron microscopy (TEM) and EDX were performed using Tecnai G2 20 TEM with an accelerating voltage of 200 kV equipped with an EDX detector. EDX elemental analysis was analyzed with TEM Image and ES Vision V4.1 analysis software and the data was averaged over at least 3 locations. The nanocrystals solvated in toluene were drop cast directly onto a carbon coated copper TEM grid and allowed to dry. Powder X-ray diffraction (PXRD) patterns were collected on a Bruker D8 Advance diffractometer with Ni-filtered Cu Kα radiation and further analysis was done using JCPDS database. The sample was drop cast and allowed to dry directly on a glass slide as the amount being used was minute. Luminescence lifetime decays were collected using time correlated single photon counting (TCSPC) using Edinburgh Instruments FLSP920. A pulsed laser diode (377 nm) with a pulse repetition rate of 500 kHz was employed for the lifetime measurements. The photoluminescence (PL) emission decay was collected at the PL peak maximum for each sample. The instrument response function was measured using a Ludox scattering solution in water. All the decay profiles were fitted by using the software EI F900 V7.2.1 with a sum of two/three exponentials shown by eq 1, where the number of components $n = 2/3$ and α_i and τ_i are the amplitude and the decay time of the ith component, respectively.[58]

$$I(t) = \sum_{i=1}^{n} \alpha_i \exp(-t/\tau_i) \quad (1)$$

Mean fluorescence lifetimes $\langle\tau\rangle$ were calculated from the decay time and the pre-exponential factors using eq 2.

$$\langle\tau\rangle = \frac{\Sigma\alpha_i\tau_i}{\Sigma\alpha_i} \quad (2)$$

Single Particle Imaging. Nanocrystals were diluted in toluene and immobilized on a glass coverslip by smearing and drying before imaging. Imaging is done using custom built TIRF microscope on Olympus IX71 inverted microscope equipped with Fianium super continuum laser and Andor Neo sCMOS camera. Total internal reflection excitation is done through 60×, 1.4 NA objective with beam exiting at greater than critical angle.[59] Excitation light is selected though bandpass filter of 460−495 nm, shell emission is collected with bandpass filter 510−550 nm (shown as green colored particles in the images), and core emission is collected through 575−675 nm (shown as red colored particles in the images). Colocalization imaging is done at the same position by changing filters manually. Images were acquired with 50 ms exposure for 5−28 s and further analyzed. In total, 157 blinking particles from 10 videos were analyzed.

CdSe Synthesis. CdSe nanocrystals were synthesized by previously reported methods in the literature.[54] A total of 0.1 mmol of CdO and 0.4 mmol of oleic acid (OA) were added to 10 mL of 1-octadecene (ODE) and heated to 280 °C with continuous stirring until a clear colorless solution was obtained. The temperature was lowered to 80 °C, and 4 g of ODA and 2 g of TOPO were added to the solution and heated again to 280 °C with continuous stirring. Subsequently, 0.1 mmol Se was dissolved in 3.5 mL of TOP at room temperature in a glovebox. This TOP-Se solution was injected swiftly into the above hot Cd solution. The temperature of the solution dropped down to 260 °C and the reaction was allowed to proceed until the desired size of the nanoparticles was achieved. The reaction was quenched by lowering the temperature with addition of room temperature toluene. The nanocrystals were purified by phase separation with a 1:1 mixture of hexane−methanol, precipitated by adding ethanol and finally redispersed in toluene. The concentration of the nanoparticles was determined by UV−vis absorption spectroscopy as described in literature.[35,60]

Stock Solutions. The Cd−oleate stock solution (0.2 M) was prepared by dissolving 0.3 mmol CdO and 2.4 mmol OA in ODE at 270 °C. A 0.2 M zinc injection solution was prepared by dissolving ZnO in 1:1 (v/v) mixture of oleic acid and TOP at 250 °C until the solution was clear. Selenium injection solution (0.2 M) was prepared by dissolving Se powder in TOP at 100 °C. Sulfur stock solution (0.2 M) was prepared by dissolving S powder in ODE at 100 °C. All the above solutions were prepared in Ar atmosphere and heated at 60 °C prior to injection.

CdSe/CdS Synthesis. A total of 2.5×10^{-7} mol of the previously prepared CdSe nanocrystals was dissolved in 3 mL of ODE and 2 g of ODA and the solution was heated to 200 °C to coat CdSe nanocrystals with a CdS shell followed by addition of required amount of Cd:S stock solutions alternately, adding enough amounts of each to cover the underlying atomic layer. The thickness of the CdS shell depends on the number of additions of Cd:S stock solutions. After completion of the CdS shell growth, the temperature of reaction mixture was increased to 250 °C and annealed for 30 min at this temperature to improve the crystallinity of the shell. The solution was cooled down to room temperature and washed twice using 1:1 mixture of hexane−methanol to remove unreacted precursors from the sample. The nanoparticles were precipitated by adding methanol, redispersed in toluene, and used for further coating of ZnSe layer over them. CdSe/CdS/ZnSe nanocrystals were synthesized by depositing a ZnSe shell around these CdSe/CdS nanocrystals.

CdSe/CdS/ZnSe Synthesis. A total of 1×10^{-7} mol of CdSe/CdS nanocrystals was dissolved in 2 mL of ODE containing 1.5 g of ODA and the solution was heated to 210 °C. The growth of the ZnSe shell is carried out by the addition of Zn:Se precursors alternately. The synthesized nanocrystals, purified by repeated washing with hexane and methanol, were redispersed in toluene and stored under an argon atmosphere.

Conflict of Interest: The authors declare no competing financial interest.

Supporting Information Available: Spectra of core/shell CdSe/mCdS nanocrystals, PL spectra of overcoating ZnSe layers on CdSe/mCdS nanocrystals, synthesis and spectra of CdS and CdS/ZnSe core/shell nanocrystals, table of lifetime data analysis and EDX results. This material is available free of charge *via* the Internet at http://pubs.acs.org.

Acknowledgment. Sameer Sapra acknowledges DRDO grant ERIPR/ER/1000389/M/01/1407 for partial financial assistance and Central Research Facility, IIT Delhi for absorption, steady state and time-resolved fluorescence. U.S., M.M., S.Y. are thankful to CSIR for research fellowship and A.P. acknowledges UGC for SRF fellowship. The authors are grateful to Sunil Jain for helping out with the single particle fluorescence microscopy. We are also thankful to Nanoscale Research Facility and Nano Science Unit of NSTI, DST for TEM facility at IIT Delhi.

REFERENCES AND NOTES

1. Greenham, N.; Peng, X.; Alivisatos, A. Charge Separation and Transport in Conjugated-Polymer/Semiconductor-Nanocrystal Composites Studied by Photoluminescence Quenching and Photoconductivity. *Phys. Rev. B* **1996**, *54*, 17628–17637.
2. Shirasaki, Y.; Supran, G. J.; Bawendi, M. G.; Bulović, V. Emergence of Colloidal Quantum-Dot Light-Emitting Technologies. *Nat. Photonics* **2012**, *7*, 13–23.
3. Ahmad, R.; Arora, V.; Srivastava, R.; Sapra, S.; Kamalasanan, M. N. Enhanced Performance of Organic Photovoltaic Devices by Incorporation of Tetrapod-Shaped CdSe Nanocrystals in Polymer-Fullerene Systems. *Phys. Status Solidi A* **2013**, *210*, 785–790.
4. Singh, G.; Zaidi, N. H.; Soni, U.; Gautam, M.; Jackeray, R.; Singh, H.; Sapra, S. Detection of Bioconjugated Quantum Dots Passivated with Different Ligands for Bio-Applications. *J. Nanosci. Nanotechnol.* **2011**, *11*, 3834–3842.
5. Sharma, A.; Pandey, C. M.; Matharu, Z.; Soni, U.; Sapra, S.; Sumana, G.; Pandey, M. K.; Chatterjee, T.; Malhotra, B. D. Nanopatterned Cadmium Selenide Langmuir–Blodgett Platform for Leukemia Detection. *Anal. Chem.* **2012**, *84*, 3082–3089.
6. Talapin, D. V.; Lee, J.-S.; Kovalenko, M. V.; Shevchenko, E. V. Prospects of Colloidal Nanocrystals for Electronic and Optoelectronic Applications. *Chem. Rev.* **2010**, *110*, 389–458.
7. Reiss, P.; Protière, M.; Li, L. Core/Shell Semiconductor Nanocrystals. *Small* **2009**, *5*, 154–168.
8. Ivanov, S. A.; Piryatinski, A.; Nanda, J.; Tretiak, S.; Zavadil, K. R.; Wallace, W. O.; Werder, D.; Klimov, V. I. Type-II Core/Shell CdS/ZnSe Nanocrystals: Synthesis, Electronic Structures, and Spectroscopic Properties. *J. Am. Chem. Soc.* **2007**, *129*, 11708–11719.
9. Blackman, B.; Battaglia, D.; Peng, X. Bright and Water-Soluble Near IR-Emitting CdSe/CdTe/ZnSe Type-II/Type-I Nanocrystals, Tuning the Efficiency and Stability by Growth. *Chem. Mater.* **2008**, *20*, 4847–4853.
10. Costi, R.; Saunders, A. E.; Banin, U. Colloidal Hybrid Nanostructures: A New Type of Functional Materials. *Angew. Chem.,Int. Ed.* **2010**, *49*, 4878–4897.
11. Yang, H.; Fan, W.; Vaneski, A.; Susha, A. S.; Teoh, W. Y.; Rogach, A. L. Heterojunction Engineering of CdTe and CdSe Quantum Dots on TiO_2 Nanotube Arrays: Intricate Effects of Size-Dependency and Interfacial Contact on Photoconversion Efficiencies. *Adv. Funct. Mater.* **2012**, *22*, 2821–2829.
12. Sharma, A.; Pandey, C. M.; Sumana, G.; Soni, U.; Sapra, S.; Srivastava, A. K.; Chatterjee, T.; Malhotra, B. D. Chitosan Encapsulated Quantum Dots Platform for Leukemia Detection. *Biosens. Bioelectron.* **2012**, *38*, 107–113.
13. Kim, S.; Fisher, B.; Eisler, H.-J.; Bawendi, M. Type-II Quantum Dots: CdTe/CdSe(Core/Shell) and CdSe/ZnTe(Core/Shell) Heterostructures. *J. Am. Chem. Soc.* **2003**, *125*, 11466–11467.
14. Ning, Z.; Tian, H.; Yuan, C.; Fu, Y.; Qin, H.; Sun, L.; Ågren, H. Solar Cells Sensitized with Type-II ZnSe–CdS Core/Shell Colloidal Quantum Dots. *Chem. Commun.* **2011**, *47*, 1536.
15. Niu, J. Z.; Shen, H.; Zhou, C.; Xu, W.; Li, X.; Wang, H.; Lou, S.; Du, Z.; Li, L. S. Controlled Synthesis of High Quality Type-II/Type-I CdS/ZnSe/ZnS Core/Shell1/Shell2 Nanocrystals. *Dalton Trans.* **2010**, *39*, 3308.
16. Chen, O.; Zhao, J.; Chauhan, V. P.; Cui, J.; Wong, C.; Harris, D. K.; Wei, H.; Han, H.-S.; Fukumura, D.; Jain, R. K.; *et al.* Compact High-Quality CdSe–CdS Core–Shell Nanocrystals with Narrow Emission Linewidths and Suppressed Blinking. *Nat. Mater.* **2013**, *12*, 445–451.
17. Nan, W.; Niu, Y.; Qin, H.; Cui, F.; Yang, Y.; Lai, R.; Lin, W.; Peng, X. Crystal Structure Control of Zinc-Blende CdSe/CdS Core/Shell Nanocrystals: Synthesis and Structure-Dependent Optical Properties. *J. Am. Chem. Soc.* **2012**, *134*, 19685–19693.
18. Nizamoglu, S.; Demir, H. V. Onion-like (CdSe)ZnS/CdSe/ZnS Quantum-Dot-Quantum-Well Heteronanocrystals for Investigation of Multi-Color Emission. *Opt. Express* **2008**, *16*, 3515.
19. Nemchinov, A.; Kirsanova, M.; Hewa-Kasakarage, N. N.; Zamkov, M. Synthesis and Characterization of Type II ZnSe/CdS Core/Shell Nanocrystals. *J. Phys. Chem. C* **2008**, *112*, 9301–9307.
20. Chen, Y.; Vela, J.; Htoon, H.; Casson, J. L.; Werder, D. J.; Bussian, D. A.; Klimov, V. I.; Hollingsworth, J. A. "Giant" Multishell CdSe Nanocrystal Quantum Dots with Suppressed Blinking. *J. Am. Chem. Soc.* **2008**, *130*, 5026–5027.
21. Tessier, M. D.; Javaux, C.; Maksimovic, I.; Loriette, V.; Dubertret, B. Spectroscopy of Single CdSe Nanoplatelets. *ACS Nano* **2012**, *6*, 6751–6758.
22. Li, J. J.; Wang, Y. A.; Guo, W.; Keay, J. C.; Mishima, T. D.; Johnson, M. B.; Peng, X. Large-Scale Synthesis of Nearly Monodisperse CdSe/CdS Core/Shell Nanocrystals Using Air-Stable Reagents *via* Successive Ion Layer Adsorption and Reaction. *J. Am. Chem. Soc.* **2003**, *125*, 12567–12575.
23. Battaglia, D.; Blackman, B.; Peng, X. Coupled and Decoupled Dual Quantum Systems in One Semiconductor Nanocrystal. *J. Am. Chem. Soc.* **2005**, *127*, 10889–10897.
24. Sapra, S.; Mayilo, S.; Klar, T. A.; Rogach, A. L.; Feldmann, J. Bright White-Light Emission from Semiconductor Nanocrystals: By Chance and by Design. *Adv. Mater.* **2007**, *19*, 569–572.
25. Dias, E. A.; Grimes, A. F.; English, D. S.; Kambhampati, P. Single Dot Spectroscopy of Two-Color Quantum Dot/Quantum Shell Nanostructures. *J. Phys. Chem. C* **2008**, *112*, 14229–14232.
26. Kostic, R.; Stojanovic, D. Multi-Color Emission in Quantum-Dot-Quantum-Well Semiconductor Heteronanocrystals. *Acta Phys. Pol., A* **2009**, *116*, 598–602.
27. SalmanOgli, A.; Rostami, A. Investigation of Electronic and Optical Properties of (CdSe/ZnS/CdSe/ZnS) Quantum Dot–Quantum Well Heteronanocrystal. *J. Nanopart. Res.* **2010**, *13*, 1197–1205.
28. Sahin, M.; Nizamoglu, S.; Yerli, O.; Volkan Demir, H. Reordering Orbitals of Semiconductor Multi-Shell Quantum Dot-Quantum Well Heteronanocrystals. *J. Appl. Phys.* **2012**, *111*, 023713.
29. Deutsch, Z.; Schwartz, O.; Tenne, R.; Popovitz-Biro, R.; Oron, D. Two-Color Antibunching from Band-Gap Engineered Colloidal Semiconductor Nanocrystals. *Nano Lett.* **2012**, *12*, 2948–2952.
30. Dinger, A.; Petillon, S.; Grün, M.; Hetterich, M.; Klingshirn, C. Conduction Band Offset of the CdS/ZnSe Heterostructure. *Semicond. Sci. Technol.* **1999**, *14*, 595–598.
31. Wei, S.-H.; Zunger, A. Calculated Natural Band Offsets of All II–VI and III–V Semiconductors: Chemical Trends and the Role of Cation *d* Orbitals. *Appl. Phys. Lett.* **1998**, *72*, 2011.
32. Brovelli, S.; Schaller, R. D.; Crooker, S. A.; García-Santamaría, F.; Chen, Y.; Viswanatha, R.; Hollingsworth, J. A.; Htoon, H.; Klimov, V. I. Nano-Engineered Electron–Hole Exchange Interaction Controls Exciton Dynamics in Core–Shell Semiconductor Nanocrystals. *Nat. Commun.* **2011**, *2*, 280.
33. Peng, X.; Schlamp, M. C.; Kadavanich, A. V.; Alivisatos, A. P. Epitaxial Growth of Highly Luminescent CdSe/CdS Core/Shell Nanocrystals with Photostability and Electronic Accessibility. *J. Am. Chem. Soc.* **1997**, *119*, 7019–7029.
34. Mooney, J.; Krause, M. M.; Saari, J. I.; Kambhampati, P. Challenge to the Deep-Trap Model of the Surface in Semiconductor Nanocrystals. *Phys. Rev. B* **2013**, *87*, 081201(R).
35. Yu, W. W.; Qu, L.; Guo, W.; Peng, X. Experimental Determination of the Extinction Coefficient of CdTe, CdSe, and CdS Nanocrystals. *Chem. Mater.* **2003**, *15*, 2854–2860.

36. Tyagi, P.; Kambhampati, P. Independent Control of Electron and Hole Localization in Core/Barrier/Shell Nanostructures. *J. Phys. Chem. C* **2012**, *116*, 8154–8160.
37. Schooss, D.; Mews, A.; Eychmüller, A.; Weller, H. Quantum-Dot Quantum Well CdS/HgS/CdS: Theory and Experiment. *Phys. Rev. B* **1994**, *49*, 17072–17078.
38. Dias, E. A.; Sewall, S. L.; Kambhampati, P. Light Harvesting and Carrier Transport in Core/Barrier/Shell Semiconductor Nanocrystals. *J. Phys. Chem. C* **2007**, *111*, 708–713.
39. Dias, E. A.; Saari, J. I.; Tyagi, P.; Kambhampati, P. Improving Optical Gain Performance in Semiconductor Quantum Dots via Coupled Quantum Shells. *J. Phys. Chem. C* **2012**, *116*, 5407–5413.
40. Bleuse, J.; Carayon, S.; Reiss, P. Optical Properties of Core/Multishell CdSe/Zn(S,Se) Nanocrystals. *Phys. E)* **2004**, *21*, 331–335.
41. Choi, C. L.; Li, H.; Olson, A. C. K.; Jain, P. K.; Sivasankar, S.; Alivisatos, A. P. Spatially Indirect Emission in a Luminescent Nanocrystal Molecule. *Nano Lett.* **2011**, *11*, 2358–2362.
42. Efros, A.; Rosen, M. Random Telegraph Signal in the Photoluminescence Intensity of a Single Quantum Dot. *Phys. Rev. Lett.* **1997**, *78*, 1110–1113.
43. Galland, C.; Ghosh, Y.; Steinbrück, A.; Hollingsworth, J. A.; Htoon, H.; Klimov, V. I. Lifetime Blinking in Nonblinking Nanocrystal Quantum Dots. *Nat. Commun.* **2012**, *3*, 908.
44. Demir, H. V.; Nizamoglu, S.; Mutlugun, E.; Ozel, T.; Sapra, S.; Gaponik, N.; Eychmüller, A. Tuning Shades of White Light with Multi-Color Quantum-Dot–Quantum-Well Emitters Based on Onion-like CdSe–ZnS Heteronanocrystals. *Nanotechnology* **2008**, *19*, 335203.
45. Nizamoglu, S.; Mutlugun, E.; Özel, T.; Demir, H. V.; Sapra, S.; Gaponik, N.; Eychmüller, A. Dual-Color Emitting Quantum-Dot-Quantum-Well CdSe-ZnS Heteronanocrystals Hybridized on InGaN/GaN Light Emitting Diodes for High-Quality White Light Generation. *Appl. Phys. Lett.* **2008**, *92*, 113110.
46. Sewall, S.; Franceschetti, A.; Cooney, R.; Zunger, A.; Kambhampati, P. Direct Observation of the Structure of Band-Edge Biexcitons in Colloidal Semiconductor CdSe Quantum Dots. *Phys. Rev. B* **2009**, *80*, 081310(R).
47. Liptay, T.; Marshall, L.; Rao, P.; Ram, R.; Bawendi, M. Anomalous Stokes Shift in CdSe Nanocrystals. *Phys. Rev. B* **2007**, *76*, 155314.
48. Talapin, D. V.; Koeppe, R.; Götzinger, S.; Kornowski, A.; Lupton, J. M.; Rogach, A. L.; Benson, O.; Feldmann, J.; Weller, H. Highly Emissive Colloidal CdSe/CdS Heterostructures of Mixed Dimensionality. *Nano Lett.* **2003**, *3*, 1677–1681.
49. Patterson, A. The Scherrer Formula for X-Ray Particle Size Determination. *Phys. Rev.* **1939**, *56*, 978–982.
50. Xia, X.; Liu, Z.; Du, G.; Li, Y.; Ma, M. Wurtzite and Zinc-Blende CdSe Based Core/Shell Semiconductor Nanocrystals: Structure, Morphology and Photoluminescence. *J. Lumin.* **2010**, *130*, 1285–1291.
51. Rawalekar, S.; Kaniyankandy, S.; Verma, S.; Ghosh, H. N. Effect of Surface States on Charge-Transfer Dynamics in Type II CdTe/ZnTe Core–Shell Quantum Dots: A Femtosecond Transient Absorption Study. *J. Phys. Chem. C* **2011**, *115*, 12335–12342.
52. Fitzmorris, B. C.; Cooper, J. K.; Edberg, J.; Gul, S.; Guo, J.; Zhang, J. Z. Synthesis and Structural, Optical, and Dynamic Properties of Core/Shell/Shell CdSe/ZnSe/ZnS Quantum Dots. *J. Phys. Chem. C* **2012**, *116*, 25065–25073.
53. Kloepfer, J. A.; Bradforth, S. E.; Nadeau, J. L. Photophysical Properties of Biologically Compatible CdSe Quantum Dot Structures. *J. Phys. Chem. B* **2005**, *109*, 9996–10003.
54. Pal, A.; Srivastava, S.; Gupta, R.; Sapra, S. Electron Transfer from CdSe-ZnS Core-Shell Quantum Dots to Cobalt(III) Complexes. *Phys. Chem. Chem. Phys.* **2013**, *15*, 15888–15895.
55. Li, J. J.; Tsay, J. M.; Michalet, X.; Weiss, S. Wavefunction Engineering: From Quantum Wells to Near-Infrared Type-II Colloidal Quantum Dots Synthesized by Layer-by-Layer Colloidal Epitaxy. *Chem. Phys.* **2005**, *318*, 82–90.
56. Panda, S. K.; Hickey, S. G.; Waurisch, C.; Eychmüller, A. Gradated Alloyed CdZnSe Nanocrystals with High Luminescence Quantum Yields and Stability for Optoelectronic and Biological Applications. *J. Mater. Chem.* **2011**, *21*, 11550.
57. Wang, X.; Ren, X.; Kahen, K.; Hahn, M. A.; Rajeswaran, M.; Maccagnano-Zacher, S.; Silcox, J.; Cragg, G. E.; Efros, A. L.; Krauss, T. D. Non-Blinking Semiconductor Nanocrystals. *Nature* **2009**, *459*, 686–689.
58. Lakowicz, J. R. *Principles of Fluorescence Spectroscopy*; 3rd ed.; Springer: New York, 2006.
59. Axelrod, D. Total Internal Reflection Fluorescence Microscopy in Cell Biology. *Traffic* **2001**, *2*, 764–774.
60. Soni, U.; Sapra, S. The Importance of Surface in Core–Shell Semiconductor Nanocrystals. *J. Phys. Chem. C* **2010**, *114*, 22514–22518.